ACS APPLIED MATERIALS & INTERFACES

Research Article

www.acsami.org

Facile Synthesis of $BaTiO_3$ Nanotubes and Their Microwave Absorption Properties

Yao-Feng Zhu,[†] Li Zhang,[‡] Toshiaki Natsuki,[§] Ya-Qin Fu,[∇] and Qing-Qing Ni*[,§,∇]

[†]Interdisciplinary Graduate School of Science and Technology, Shinshu University, Tokida, Ueda 386-8576, Japan

[‡]Faculty of Engineering, Shinshu University, Wakasato, Nagano 380-8553, Japan

[§]Department of Functional Machinery & Mechanics, Shinshu University, Tokida, Ueda 386-8576, Japan

[∇]Key Laboratory of Advanced Textile Materials and Manufacturing Technology Ministry of Education, Zhejiang Sci-Tech University, Hangzhou 310018, People's Republic of China

ABSTRACT: Uniform $BaTiO_3$ nanotubes were synthesized via a simple wet chemical route at low temperature (50 °C). The as-synthesized $BaTiO_3$ nanotubes were characterized using powder X-ray diffraction, field-emission scanning electron microscopy, transmission electron microscopy, Raman spectroscopy, and X-ray photoelectron spectroscopy. The results show that the $BaTiO_3$ nanotubes formed a cubic phase with an average diameter of ∼10 nm and wall thickness of 3 nm at room temperature. The composition of the mixed solvent (ethanol and deionized water) was a key factor in the formation of these nanotubes; we discuss possible synthetic mechanisms. The microwave absorption properties of the $BaTiO_3$ nanotubes were studied at microwave frequencies between 0.5 and 15 GHz. The minimum reflection loss of the $BaTiO_3$ nanotubes/paraffin wax composite ($BaTiO_3$ nanotubes weight fraction = 70%) reached 21.8 dB (∼99.99% absorption) at 15 GHz, and the frequency bandwidth less than −10 dB is from 13.3 to 15 GHz. The excellent absorption property of $BaTiO_3$ nanotubes at high frequency indicates that these nanotubes could be promising microwave-absorbing materials.

KEYWORDS: *$BaTiO_3$ nanotubes, crystal structure, morphology, microwave absorption*

INTRODUCTION

Nanostructure materials currently are under intensive investigation, because of their unique shape- and size-dependent properties, as well as their potential applications as advanced materials with collective properties.[1,2] Among the different morphologies of nanomaterials, one-dimensional (1D) nanostructures have received considerable attention from the scientific community, and they have been investigated extensively in a variety of application, such as electronics, optoelectronics, mechanics, catalysis, and biological and environmental systems, because of their unique physical and chemical properties, particularly their smaller size and large specific surface area.[3,4] Moreover, one-dimensional nanostructure is considered an ideal form for the fabrication of devices.

Barium titanate ($BaTiO_3$) perovskite is famous for its high dielectric constant and ferroelectric response, both of which are regarded as being quite useful in the electronics industry as multilayer ceramic capacitors, thermistors and piezoelectric transducers, electro-optical applications, photonic crystals, ceramics, and microwave absorbers, to name a few.[5,6] With a wide range of applications, the synthesis and characterization of the one-dimensional (1D) $BaTiO_3$ nanostructure provides strong motivation to understand its properties.

However, to the best of our knowledge, the traditional techniques for preparing $BaTiO_3$ nanostructures rely on high pressure or high temperature, as in, for instance, classical solid-state routes,[7] the hydrothermal route,[8] and the sol−gel method.[9] Bao et al. prepared a variety of nanostructured such as nanocubes, coral-like nanostructures, and starfish-like nanostructures through hydrothermal synthesis.[1] Tian et al. reported that $BaTiO_3$ hollow nanoparticles were obtained through a one-pot template-free route in a molten hydrated salt medium.[10] In contrast, relatively few studies on the synthesis of $BaTiO_3$ nanotubes are available in the literature. Therefore, seeking a simple method for a low-cost, lower-temperature, and large-scale preparation of $BaTiO_3$ nanotubes with fine crystallinity and high purity remains a severe challenge. Moreover, there have been few investigations specifically concerned with $BaTiO_3$ as a microwave absorber. $BaTiO_3$ is a type of dielectric material; relaxation present in $BaTiO_3$ occurs at gigahertz (GHz) frequencies, which can be characterized by a decrease in dielectric constant (ε) and a peak in the dielectric loss (tan δ) with increasing frequency. Thus, it is natural to speculate that $BaTiO_3$ might be useful as a microwave absorber.[11,12] On the other hand, the small diameters of nanotubes with hollow structure and high interface areas, which result in an increase of the absorption points, and the microwaves can be trapped by the hollow structures for longer periods, creating conditions for microwave energy loss. Therefore, these features make the synthesis of $BaTiO_3$ nanotubes as a microwave absorber a very promising work.

In this work, we report the facile synthesis of $BaTiO_3$ nanotubes in ethanol/water mixed solvent at low temperature (∼50 °C). The structure, morphology, and possible mechanism of formation of $BaTiO_3$ nanotubes are discussed. Microwave

Received: January 13, 2012
Accepted: March 12, 2012
Published: March 12, 2012

   dx.doi.org/10.1021/am300069x | ACS Appl. Mater. Interfaces 2012, 4, 2101−2106

and absorption properties were also investigated and results are presented.

EXPERIMENTAL SECTION

Materials. Titania (P25) was obtained from Degussa (Germany). Barium hydroxide octahydrate, sodium hydroxide, formic acid, hydrochloric acid and ethanol were supplied by Wako Pure Chemical Reagent Co., Ltd. (Japan). All chemicals were used without further purification.

Hydrothermal Synthesis of H_2TiO_3 Nanotubes. H_2TiO_3 nanotubes (abbreviated hereafter as HTO) were prepared by a simple hydrothermal method, according to previous work with some modification.[13] In a typical procedure, 0.5 g of TiO_2 powder was added to 50 mL of 10 M NaOH aqueous solution and magnetic stirred at room temperature for 12 h. Next the mixed suspension was transferred into Teflon-lined autoclave, and the autoclave was then sealed and placed in an oven and heated to 150 °C, for 48 h. The newly formed white suspension was separated from the liquid by centrifuge and washed with deionized water and aged in an aqueous of 0.1 M HCL solution to exchange Na^+ with H^+. Afterward, the treated powder was filtered and washed repeatedly with distilled water until the pH level was almost neutral. Finally, the resulting white precipitates were dried under vacuum at 50 °C for 24 h.

Synthesis of $BaTiO_3$ Nanotubes. $BaTiO_3$ nanotubes were prepared using a simple wet chemical route. The prepared HTO was added to ethanol/water mixed solvent with 25% ethanol by volume, and sonicated for 10 min to break up any agglomeration. Next, $Ba(OH)_2{\cdot}8H_2O$ was added to the prepared suspension in a beaker; afterward, the beaker was put into a 50 °C water bath for 4 h under magnetic stirring. The molar ratio of Ba^{2+} to Ti^{4+} was 1:1. After the reaction was completed, the beaker was taken out. The resulting products were washed sequentially with 0.1 M formic acid, ethanol, and distilled water. Finally, the final product was dried under vacuum at 50 °C overnight for further characterization.

Characterization. The crystal structure of the prepared powders was analyzed with a diffractometer (RINT, Model 2550H), using Cu Kα radiation. Raman spectroscopy was also used to investigate the existing phase of the synthesized powders with HoloLab series 5000 Raman spectroscopy system (514-nm excitation of the laser). The morphology and microstructure of the products were characterized using field-emission scanning electron microscopy (FE-SEM) (JEOL, Model S-5000) and transmission electron microscopy (TEM) (JEOL, Model JEM-2010) with an accelerating voltage of 200 kV. X-ray photoelectron spectroscopy (XPS) analysis (Kratos AXIS Ultra DLD) was used to measure the elemental composition of the samples.

The real and imaginary parts of the complex permittivity ε ($\varepsilon = \varepsilon' - j\varepsilon''$) and permeability μ ($\mu = \mu' - j\mu''$) were measured using a vector network analyzer (37247D Anritsu Co., Ltd.) over a range of 0.5−15 GHz. For this, samples were prepared with $BaTiO_3$ loading in paraffin. The weight percentage of $BaTiO_3$ to paraffin was varied from 40% to 70%. The powder−wax compound was pressed into a toroidal shape with an outer diameter of 7 mm, an inner diameter of 3.0 mm, and a thickness of 2 mm.

RESULTS AND DISCUSSION

Structure and Morphology Analysis. Figure 1 presents the X-ray diffraction (XRD) patterns of the as-prepared $BaTiO_3$ nanotubes synthesized by the simple wet chemical route. All diffraction peaks can be labeled and assigned to the cubic crystal structure of $BaTiO_3$, and the lattice constant is indexed as a = 4.031 Å; b = 4.031 Å; c = 4.031 Å; thus, there is no indication of crystalline byproducts such as TiO_2 or $BaCO_3$, which matches well with the reported data (JCPDS Powder Diffraction File Card No. 31-0174). The thermodynamically stable polymorph of bulk $BaTiO_3$, in contrast, has a noncentrosymmetric tetragonal phase that is ferroelectric at room temperature.[14,15]

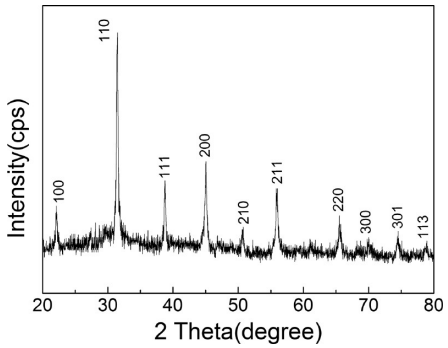

Figure 1. XRD pattern of $BaTiO_3$ nanotubes.

Representative FE-SEM images of HTO nanotubes and $BaTiO_3$ nanotubes are shown in Figures 2a−d. Figures 2a and

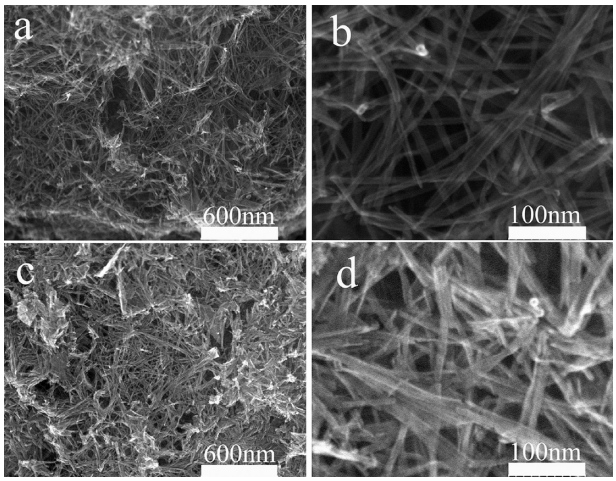

Figure 2. Representative FE-SEM images of (a, b) HTO nanotubes and (c, d) $BaTiO_3$ nanotubes.

2c are low-magnification images of HTO and $BaTiO_3$ nanotubes, respectively. Indicatively, the $BaTiO_3$ product has a morphology that is similar to that of HTO nanotubes, which mainly has a homogeneous structure over the large scale; this is further confirmed by TEM images. The length of the nanotubes is several hundred nanometers to several micrometers. The high-magnification images of HTO and $BaTiO_3$ nanotubes (Figures 2b and 2d, respectively) demonstrate that the as-prepared nanotubes have a uniform diameter of ∼10 nm.

Further structural characterization was performed by TEM, from which images of the $BaTiO_3$ nanotubes at different resolutions are shown in Figures 3a−c. Figures 3a and 3b reveal that the $BaTiO_3$ one-dimensional (1D) nanomaterials have a hollow structure typical of nanotubes, hence the use of the term. The $BaTiO_3$ nanotubes have a mean diameter and wall thickness of ∼10 and 3 nm, respectively, as measured from TEM images; that is in accordance with the FE-SEM observations obtained from Figure 2. The selected-area electron diffraction pattern (SAED) for the cubic $BaTiO_3$ nanotubes presented in Figure 3d enables $BaTiO_3$ to be indexed as a cubic $Pm\bar{3}m$ space group, using the $BaTiO_3$ unit cell parameters (JCPDS Powder Diffraction File Card No. 31-0174) and the single-crystal nature of $BaTiO_3$ nanotubes. The representative high-resolution TEM image of the nanotube in Figure 3c further reveals that $BaTiO_3$ nanotubes form a single crystal with

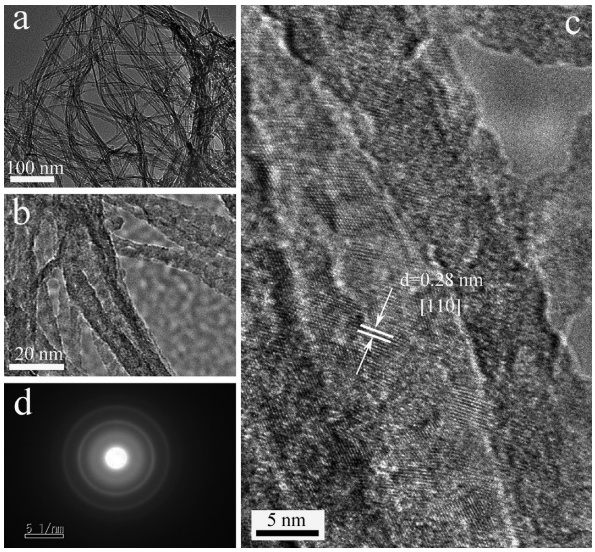

Figure 3. (a, b, and c) TEM images of the $BaTiO_3$ nanotubes at different resolutions. (d) Selected-area electron diffraction (SAED) pattern of $BaTiO_3$ nanotubes.

an interplanar crystal spacing of ~0.28 nm that corresponds to the (110) crystalline plane.

Raman spectroscopy is generally a highly sensitive spectroscopic technique to probe structure at the atomic scale on the basis of vibrational symmetry. Cubic $BaTiO_3$ inherently has no Raman-active modes, but such modes are expected for the noncentrosymmetric tetragonal structure.[16,17] The Raman spectrum of the $BaTiO_3$ nanotubes is shown in Figure 4. The observed Raman peaks have been assigned to

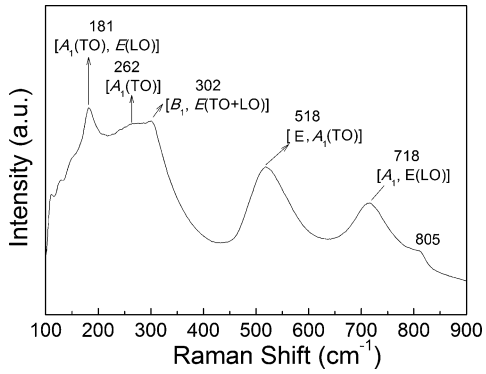

Figure 4. Raman spectrum of the $BaTiO_3$ nanotubes.

more than one phonon mode, where, in the Raman spectra of the $BaTiO_3$ nanotubes, sharp bands at ~181 cm^{-1} [A_1(TO), E(LO)] and 302 cm^{-1} [B_1, E(TO+LO)] and broad bands at ~262 cm^{-1} [A_1(TO)], 518 cm^{-1} [E, A_1 (TO)], and 718 cm^{-1} [A_1, E(LO)], all of which are suggestive of a tetragonal phase.[5,9] Even though XRD analysis reveals a cubic perovskite structure, the observed Raman-active modes imply a certain degree of tetragonality on the atomic scale, in accordance with the previous report.[9] The peak at 805 cm^{-1} is not an intrinsic mode of tetragonal $BaTiO_3$;[18] it may be associated with the presence of hydroxyl lattice groups, which can reside as defects on oxygen sites with $BaTiO_3$.[19,20]

To verify the composition of the nanotube and confirm the chemical states of the elements, we performed XPS, the spectra from which are presented in Figure 5. Survey scans of the sample identified the presence mainly of barium (Ba 3d, 4s, 4p,

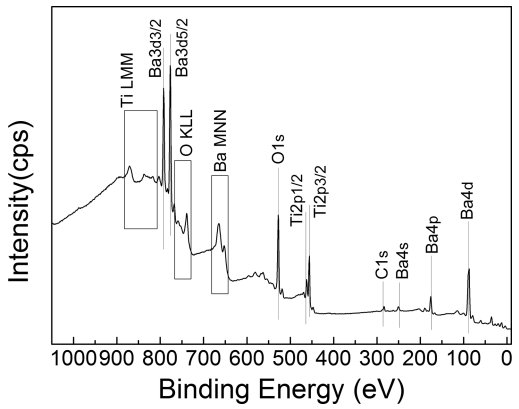

Figure 5. X-ray photoelectron spectroscopy (XPS) spectrum of the $BaTiO_3$ nanotubes.

4d), titanium (Ti 2p), and oxygen (O 1s). The Ba $3d_{5/2}$ and Ti $2p_{3/2}$ binding energies measured for the nanotubes were 777.8 and 456.9 eV, respectively, which is in good agreement with those reported.[9] Moreover, the ratio of Ti:Ba is ~1.07, calculated by the peak area of Ba 3d and Ti 2p, which indicated that the product has relatively high purity. Nevertheless, trace amounts of carbon element were revealed in the spectra. A residual carbon content of ~2.21 wt % was calculated according to the peak area, presumably remaining organic solvents of formic acid and ethanol, or contamination from the carbon conductive tape in the process of test sample preparation. Moreover, no CO^{3-} impurity was detected by either XRD or Raman spectroscopy.

To probe the formation mechanism of single-crystalline $BaTiO_3$ nanotubes under reaction system of ethanol/water mixed solvent at low temperature, a series of experiments were performed. The reaction system of mixed solvent might play important role in the growth of $BaTiO_3$ nanotubes. Figures 6a and 6b show typical FE-SEM images of $BaTiO_3$ powders prepared by different volume ratios of ethanol/water mixed solvent. If prepared with mixed solvent with 10% ethanol by volume and heated at 50 °C for 4 h, the obtained sample consisted of $BaTiO_3$ nanotubes. However, with mixed solvent with 50% ethanol by volume, the product obtained consisted of $BaTiO_3$ nanoparticles, not nanotubes. In addition, the XRD analysis indicated that the as-prepared $BaTiO_3$ phase well-crystallized with increasing ethanol volume (see Figure 6c). According to the results, the possible formation mechanism of $BaTiO_3$ nanotubes might be dominated by topochemical reactions (as shown in Figure 7).[21−23] The Ba^{2+} species in the solution can react initially with HTO nanotubes to form a Ba-doping H_2TiO_3 layer on the surface of HTO nanotubes. Moreover, with similar crystallographic features of $BaTiO_3$ and HTO, and the thin walls of HTO nanotubes, the propagation of the reaction was expected to occur more easily along the entire HTO nanotubes, which were transformed to $BaTiO_3$, through reaction with barium ions (Ba^{2+}) or complexes ($BaOH^+$) that continuously diffused through the outside $BaTiO_3$ layer, and finally $BaTiO_3$ nanotube crystallites were formed. This process was possible even at low temperatures, because of the supersaturation caused by the lowered dielectric constant (ε) of the mixed solvent ($\varepsilon_{ethanol}$ = 25, ε_{water} = 80).[24,25]

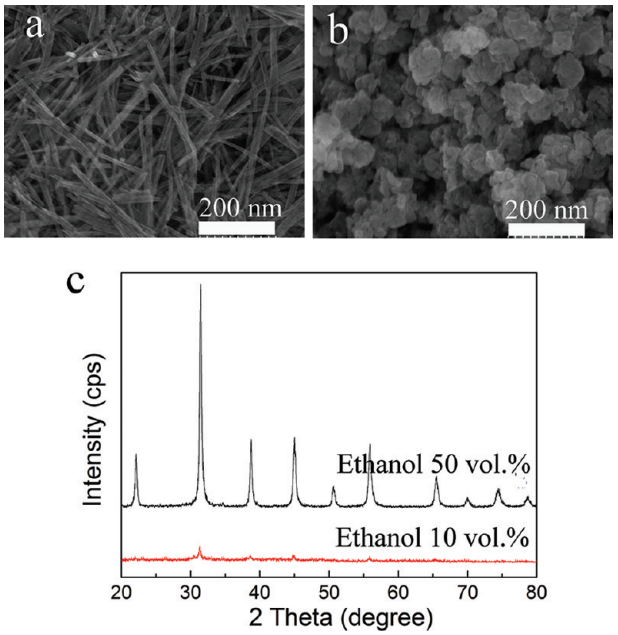

Figure 6. Typical FE-SEM images of the powders prepared by different volume ratio of ethanol/water mixed solvent: (a) mixed solvent with 10% ethanol by volume; (b) mixed solvent with 50% ethanol by volume; and (c) XRD patterns of the powders prepared by different ethanol/water mixed solvent volume ratios.

However, with mixed solvent with 50% ethanol by volume used as the reaction system, the product obtained consisted of $BaTiO_3$ nanoparticles, which occur for the reason of the relatively low dielectric constant makes the solution more supersaturated, which can increase the nucleation rate.[24] Therefore, the dissolved parts of H_2TiO_3 react with barium or complexes in solution, forming $BaTiO_3$ particles via a dissolution−precipitation process.

Electromagnetic Wave Absorption Properties of $BaTiO_3$ Nanotubes. To the best of our knowledge, the microwave absorption properties of the $BaTiO_3$ nanotubes have not been studied. Here, the microwave absorption properties of the novel $BaTiO_3$ nanotubes were investigated. Figures 8a and 8b show the frequency dependence of the complex

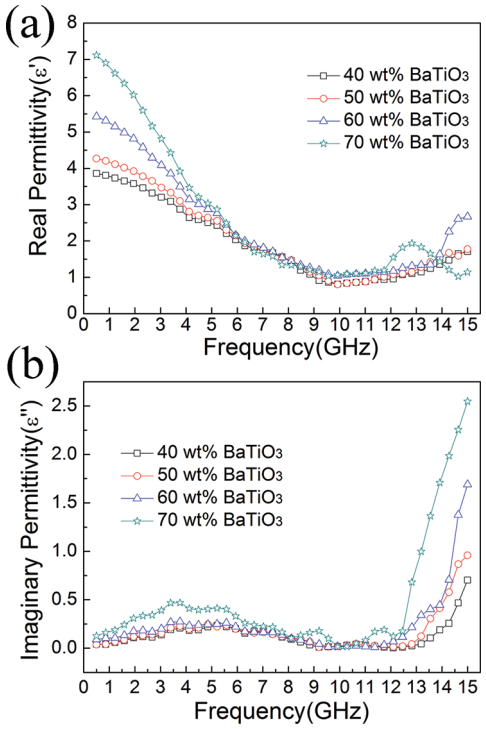

Figure 8. (a) Real part ε' and (b) imaginary part (ε'') of the complex permittivity of the mixture of $BaTiO_3$ nanotubes and paraffin wax with different weight fraction.

permittivity—the real part (ε') and the imaginary part (ε'')—of the mixture of $BaTiO_3$ nanotubes and paraffin wax with different weight fractions. The dip and slight rise with increasing frequency appearing in ε' for the samples is mainly due to the various polarizabilities (electronic, ionic, and orientation) and electric displacement of dielectric materials not keeping up with the variational microwave band.[26] As the $BaTiO_3$ weight fraction increased from 40% to 70%, ε' increased in the frequency range of 0.5−6 GHz. Since all samples have similar ε' values in the high-frequency range, this indicates that the ε' value of the samples is less sensitive to the $BaTiO_3$ content.

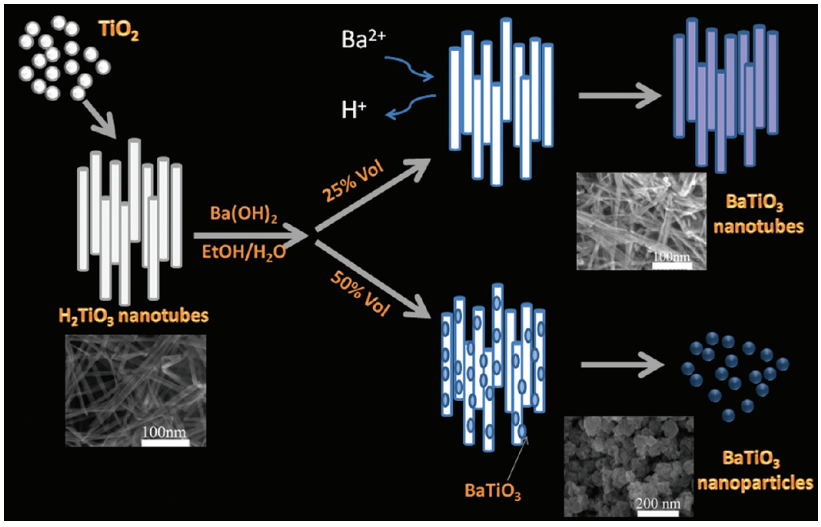

Figure 7. Schematic illustration of the formation mechanism of $BaTiO_3$ nanotubes and $BaTiO_3$ nanoparticles.

dx.doi.org/10.1021/am300069x | ACS Appl. Mater. Interfaces 2012, 4, 2101−2106

In contrast, ε'' shows an appreciable increase with increasing $BaTiO_3$ content, especially in the higher frequency range. Samples showed little change up to a frequency of 12 GHz and then increased with increasing frequency over the higher frequency range (see Figure 8b). The dielectric loss at relatively low frequency is explained as being determined by the leak conductance, whereas at relatively high frequencies, the mechanisms contributing to dielectric loss are the relaxation polarization and electric conductance.[27] More specifically, the loss mechanisms in dielectric $BaTiO_3$ are dominated mainly by dielectric polarization, spontaneous polarization, and the associated relaxation phenomena.[28]

Figures 9a and 9b show the frequency dependence of the real (μ') and imaginary (μ'') parts of the complex permeability

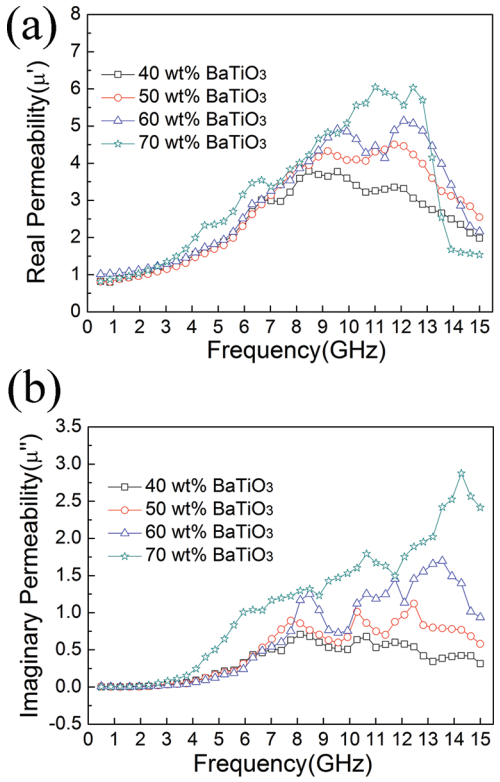

Figure 9. (a) Real part (μ') and (b) imaginary part (μ'') of complex permeability of the mixture of $BaTiO_3$ nanotubes and paraffin wax with different weight fractions.

spectra of the mixture of $BaTiO_3$ nanotubes and paraffin wax with different weight fractions. The μ' and μ'' values of samples exhibit a resonance peak in the relatively high frequency range (between 4 and 15 GHz). The resonance peak may be related to a natural resonance. However, these values are higher than previously reported;[26,29] this could be due to equipment error and must be checked by testing blank samples. Nevertheless, further study is needed to understand more of the details.

The reflection loss (RL) was calculated according to transmission line theory, as follows:

$$\mathrm{RL} = 20 \log \left| \frac{Z_{in} - 1}{Z_{in} + 1} \right| \quad (1)$$

The normalized input impedance (Z_{in}) is given by the formula

$$Z_{in} = \sqrt{\frac{\mu_r}{\varepsilon_r}} \tanh\left[j\left(\frac{2\pi f d}{c}\right)\sqrt{\mu_r \varepsilon_r} \right] \quad (2)$$

where $\varepsilon_r = \varepsilon' - j\varepsilon''$, $\mu_r = \mu' - j\mu''$, f is the microwave frequency (in Hz), d is the thickness of the absorber (in m), and c is the velocity of light in free space (in units of m/s). The reflection loss (RL) of mixtures of $BaTiO_3$ nanotubes and paraffin wax with different weight fractions were measured at a sample thickness of 2 mm, and the results are shown in Figure 10. The

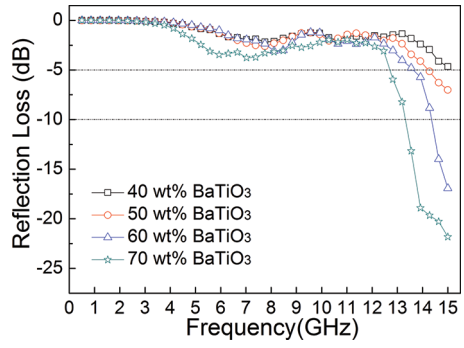

Figure 10. Reflection loss (RL) curves for $BaTiO_3$ nanotubes with a thickness of 2 mm, in the frequency range of 0.5−15 GHz.

microwave-absorbing parameter for the samples is listed in Table 1. It can be seen that the frequency for the minimum

Table 1. Microwave Absorbing Properties of Samples

	Microwave-Absorbing Properties of Sample			
sample (weight fraction of $BaTiO_3$)	minimum reflection loss value, RL_m (dB)	f_m[a] (GHz)	frequency range (GHz) (RL ← 5 dB)	frequency range (GHz) (RL ← 10 dB)
40%	4.7	15	0	0
50%	7.0	15	0.7	0
60%	16.9	15	1.50	0.65
70%	21.8	15	2.30	1.80

[a]Frequency at which the reflection loss is the minimum.

reflection loss increases as the weight fraction increases. The $BaTiO_3$ nanotubes/paraffin wax composite shows a minimum reflection loss of 21.8 dB (~99.99% absorption) at 15 GHz for a weight fraction of 70%, and the frequency bandwidth at less than −10 dB is from 13.3 GHz to 15 GHz. The minimum reflection loss of other samples is also achieved around a frequency of 15 GHz. Through analysis, the dip found at 15 GHz corresponds to a matching resonance frequency condition.[30] We note that $BaTiO_3$ nanotubes have excellent absorbing properties at high frequencies. The small diameters (~10 nm) of nanotubes lead to high interface areas, which, with a hollow structure, result in the complicated interface polarization and intensive dielectric relaxation. Moreover, increased interface areas increase the absorption points, so that microwaves can be trapped by the hollow structures for longer periods, creating conditions whereby microwave energy is transformed to heat energy or other forms of energy, and finally dissipate.[28]

CONCLUSIONS

In summary, $BaTiO_3$ nanotubes were successfully synthesized by a simple wet chemical route at low temperature. Reaction solvents were found to play a key role in the formation, with a possible mechanism being via topochemical reactions. Because of a high interface area and hollow structure, the microwave absorption of the $BaTiO_3$ nanotubes/paraffin wax composite reached a minimum reflection loss of 21.8 dB (~99.99% absorption) at 15 GHz for a weight fraction of 70%. Therefore, it is reasonable to believe that $BaTiO_3$ nanotubes can be useful materials as microwave absorbers.

AUTHOR INFORMATION

Corresponding Author

*Tel./Fax: +81 268 21 5438. E-mail: niqq@shinshu-u.ac.jp.

Notes

The authors declare no competing financial interest.

ACKNOWLEDGMENTS

This work was partly supported by grants-in-aid from the Global COE Program and CLUSTER (the second stage) by the Ministry of Education, Culture, Sports, Science and Technology, Japan.

REFERENCES

(1) Bao, N. Z.; Shen, L. M.; Srinivasan, G.; Yanagisawa, K.; Gupta, A. *J. Am. Chem. Soc.* **2008**, *112*, 8634.
(2) Yin, Y. D.; Alivisatos, A. P. *Nature* **2005**, *437*, 664.
(3) Jiang, C. L.; Kiyofumi, K.; Wang, Y. F.; Koumoto, K. *Crys. Growth Des.* **2007**, *7*, 2713.
(4) Lee, D. Y.; Lee, M. H.; Cho, N. I.; Kim, B. Y.; Oh, Y. J. *Met. Mater. Int.* **2010**, *16*, 453.
(5) Mao, Y. P.; Mao, S. Y.; Ye, Z. G.; Xie, Z. X.; Zheng, L. S. *Mater. Chem. Phys.* **2010**, *124*, 1232.
(6) Habiba, A.; Haubnerb, R.; Stelzera, N. *Mater. Sci. Eng., B* **2008**, *152*, 60.
(7) Chu, M. S. H.; Rae, A. W. I. M. *Am. Ceram. Soc. Bull.* **1995**, *74*, 69.
(8) Zhu, X. H.; Zhang, Z. H.; Zhu, J. M.; Zhou, S. H.; Liu., Z. G. *J. Cryst. Growth* **2009**, *311*, 2437.
(9) Brutchey, R. L.; Morse, D. E. *Angew. Chem.* **2006**, *118*, 6714.
(10) Tian, X. L.; Li, J.; Chen, K.; Han, J.; Pan, S. *Crys. Growth Des.* **2009**, *9*, 4927.
(11) Chen, X. D.; Wang, G. Q.; Duan, Y. P.; Liu., S. H. *J. Alloys Compd.* **2008**, *453*, 433.
(12) Chen, X. D.; Wang, G. Q.; Duan, Y. P.; Liu, S. H. *J. Phys. D: Appl. Phys.* **2007**, *40*, 1827.
(13) http://www.dtic.mil/cgi-bin/GetTRDoc?Location=U2&doc=GetTRDoc.pdf&AD=ADA480692.
(14) Kolen'ko, Y. V.; Kovnir, K. A.; Neira, I. S.; Taniguchi, T.; Ishigaki, T.; Watanabe, T.; Sakamoto, N.; Yoshimura., M. *J. Phys. Chem. C* **2007**, *111*, 7306.
(15) Adireddy, S.; Lin, C. K.; Cao, B. B.; Zhou, W. L.; Caruntu, G. *Chem. Mater.* **2010**, *22*, 1947.
(16) Asiaie, R.; Zhu, W. D.; Akbar, S. A.; Dutta, P. K. *Chem. Mater.* **1996**, *8*, 229.
(17) El Marssi, M.; Le Marrec, F.; Lukyanchuk, I. A.; Karkut, M. G. *J. Appl. Phys.* **2003**, *94*, 3309.
(18) Shiratori, Y.; Pithan, C.; Dornseiffer, J.; Waser, R. *J. Raman Spectrosc.* **2007**, *38*, 1291.
(19) Tian, X. L.; Li, J.; Chen, K.; Han, J.; Pan, S. L.; Wang, Y. J.; Fan, X. Y.; Li, F.; Zhou, Z. X. *Cryst. Growth Des.* **2010**, *10*, 3994.
(20) Joshi, U. A.; Yoon, S.; Baik, S.; Lee., J. S. *J. Phys. Chem. B* **2006**, *110*, 12252.
(21) Feng, Q.; Yanagisawa, K.; Yamasaki, N. *High Pressure Res.* **2001**, *20*, 149.
(22) Zhu, H. Y.; Gao, X. P.; Lan, Y.; Song, D. Y.; Xi, Y. X.; Zhao, J. C. *J. Am. Chem. Soc.* **2004**, *126*, 8380.
(23) Bao, N. Z.; Shen, L. M.; Srinivasan, G.; Yanagisawa, K.; Gupta, A. *J. Phys. Chem.. C* **2008**, *112*, 8634.
(24) Lee, D. K.; Cho, I. S.; Lee, S. W.; Kim, D. H.; Shim, H. W.; Kim, D. W.; Hong, K. S. *Eur. J. Inorg. Chem.* **2010**, *2010*, 1344.
(25) Puranik, S. M.; Kumbharkhane, A. C.; Mehrotra, S. C. *J. Mol. Liq.* **1994**, *59*, 173.
(26) Wang, G. Q.; Chen, X. D.; Duan, Y. P.; Liu, S. H. *J. Alloys Compd.* **2008**, *454*, 343.
(27) Kaatze, U. *Metrologia* **2010**, *47*, S91−S113.
(28) Xia, F.; Liu, J. W.; Gu, D.; Zhao, P. F.; Zhang, J.; Che, R. C. *Nanoscale* **2011**, *3*, 3865.
(29) Qing, Y. C.; Zhou, W. C.; Luo, F.; Zhu., D. M. *J. Magn. Magn. Mater.* **2011**, *323*, 602.
(30) Zou, Z.; Xuan, A. G.; Yan, Z. G.; Wu, Y. X.; Li, N. *Chem. Eng. Sci.* **2010**, *65*, 164.